Confinement and Threshold Modeling for High Temperature GeSn and GeC/GeCSn Lasers

Md. Shamim Reza, Tuhin Dey, Augustus W. Arbogast, Qian Meng, Seth R. Bank, *Fellow, IEEE*, and Mark A. Wistey, *Senior Member, IEEE*

***Abstract*—Models of GeSn and GeCSn quantum well (QW) lasers were compared to predict net gain and threshold for computing applications. GeSn showed weak confinement of electrons in both k-space (directness) and real space, as well as a weak optical confinement factor. Using material parameters from ab-initio calculations, adding 1-2% carbon to Ge or GeSn could provide all three confinements simultaneously, with up to 350 meV of electron confinement by Ge QW barriers and a direct bandgap that is 50-220 meV below the indirect gap. A 2-4x increase in electron effective mass preserves strong confinement even in narrow, 5 nm GeCSn/Ge quantum wells. Simply keeping electrons out of non-lasing, higher energy states doubles the differential gain compared with GeSn lasers and reduces free carrier absorption, while deeper QWs further enhance gain. GeCSn laser thresholds as low as 160 A/cm^2 are predicted for operation at temperatures of 100 °C, two orders of magnitude lower than comparable GeSn lasers.**

***Index Terms*—Germanium alloys, silicon photonics, diode lasers, semiconductor lasers, waveguide lasers, energy states, effective mass.**

I. Introduction

THERE is a tremendous need for on-chip lasers, amplifiers, and compact modulators on silicon for accelerators and extreme bandwidth interconnects for machine learning (ML) [1], thousand-core CPUs and GPUs [2], [3], and vector/tensor multiplication (TPUs) [4], [5]. Furthermore, most ML algorithms are dominated by vector-matrix operations such as multiply and accumulate (MAC) [6], and optical MAC could operate as fast as input fetch, potentially 100x faster than conventional electronics [7]. Also, existing passive devices for silicon photonics, such as waveguides, have lower losses than their GaAs and InP counterparts [8], but the lack of on-chip amplifiers means that optical signals can only accumulate loss as they pass through successive optical elements, closing the eye diagram. This limits fanout and hinders one-to-many applications such as shared parallel memory fetch. Active photonic interconnects using integrated lasers and semiconductor optical amplifiers (SOAs) would increase fanout, relax the memory bottleneck, and make more connections reachable within a clock cycle. This would benefit Big Data algorithms and the large networks needed for overparameterization in ML [9]. In addition, integration of direct bandgap materials on Si could reduce the size of the thousands of modulators already on photonic integrated circuits. Active photonics on Si would further enable a wide range of inexpensive applications from eye-safe LiDAR, biochemical and gas sensors, SWIR/MIR hyperspectral cameras for disaster rescue, and skin-neutral measurements of fever and blood oximetry. Unfortunately, neither Si nor any of the other Group IV elements emits usable amounts of light.

However, Ge has a nearly-direct bandgap and can be grown on Si with negligible dislocation densities even in thin layers [10], [11]. Adding tensile strain and/or alloying with Sn can push the Ge direct gap conduction band (CB) valley energy (E_Γ) below that of the L valley (E_L) to create a direct bandgap suitable for lasers. Indeed, lasers using GeSn alloys or tensile strained Ge (t-Ge) have been predicted and demonstrated, but to date, they have only operated with optical pumping or at cryogenic temperatures [12], [13], [14], [15], [16], [17], [18], [19], [20], [21], [22]. The bandgaps of GeSn and tensile Ge are universally reported to be weakly direct at best, reported as E_L-$E_\Gamma < 90$ meV, and the directness may be reduced to less than kT and even lost when confined in a quantum well (QW) [23], [24], [25], [26], [27]. Therefore, most electrons at room temperature remain in the multiple, degenerate, large-mass L valleys rather than the small-mass valley at Γ [28]. This reduces laser efficiency due to the reduced differential gain and increased free carrier absorption [29]. Several theoretical models have been used to analyze GeSn and tensile Ge laser designs [12], [23], [28], [29], [30], [31], [32], [33], but electrically pumped, room temperature GeSn lasers have remained elusive [30].

On the other hand, strong directness (E_L - $E_\Gamma > 144$ meV) is predicted for the addition of roughly 1% C to Ge or GeSn, which dramatically reduces E_Γ while leaving E_L nearly unchanged

Received 1 June 2024; revised 22 October 2024 and 27 November 2024; accepted 2 December 2024. Date of publication 4 December 2024; date of current version 20 December 2024. This work was supported in part by AFOSR under Award FA9550-23-1-0458, in part by National Science Foundation under Grant DMR-1508646, Grant DMR 1810280, CBET-1438608, and Grant PREM DMR-2122041, and in part by the Center for Dynamics and Control of Materials, with additional support from the University of Texas at Austin under Grant DMR-1720595. *(Corresponding author: Mark A. Wistey.)*

Md. Shamim Reza was with Texas State University, San Marcos, TX 78666 USA. He is now with Intel, Hillsboro, OR 97124 USA.

Tuhin Dey was with Texas State University, San Marcos, TX 78666 USA. He is now with the Lam Research, Tualatin, OR 97062 USA.

Augustus W. Arbogast is with the Physics Department, Texas State University, San Marcos, TX 78666 USA.

Qian Meng and Seth R. Bank are with the Department of Electrical and Computer Engineering, University of Texas at Austin, Austin, TX 78758 USA (e-mail: sbank@utexas.edu).

Mark A. Wistey is with the Department of Physics and the Materials Science, Engineering, and Commercialization Program, Texas State University, San Marcos, TX 78666 USA (e-mail: mwistey@txstate.edu).

This article has supplementary material provided by the authors and color versions of one or more figures available at https://doi.org/10.1109/JSTQE.2024.3511716.

Digital Object Identifier 10.1109/JSTQE.2024.3511716

1077-260X © 2024 IEEE. All rights reserved, including rights for text and data mining, and training of artificial intelligence and similar technologies. Personal use is permitted, but republication/redistribution requires IEEE permission. See https://www.ieee.org/publications/rights/index.html for more information.

Authorized licensed use limited to: Texas State University. Downloaded on May 19,2025 at 15:53:30 UTC from IEEE Xplore. Restrictions apply.

[34], [35], [36]. This greatly reduces the fraction of Sn required for a direct bandgap, which eliminates growth problems such as Sn droplets.[37] Crucially, adding 1% C does not create a defect-like state [38] with weak optical emission. Rather, band anticrossing (BAC) splits and moves the Γ conduction band valley down, so the optical transition strength in Ge:C is comparable with GaAs [39]. Furthermore, small amounts of Sn significantly enhance substitutional C while reducing C-C defects [34], [36].

This work examines the consequences of optical and carrier confinement in GeSn, $Ge_{1-x}C_x$ (GeC), and/or $Ge_{1-x-y}C_xSn_y$ (GeCSn) QW laser designs. Adding C to Ge or GeSn is predicted to offer far lower laser thresholds and electrically pumped lasing, even at CPU temperatures, by simultaneously enabling strong carrier and optical confinement. The reduced threshold current density reduces free carrier absorption, which further reduces thresholds, especially at high temperatures.

II. Methods

Threshold current densities were calculated for ridge waveguide QW lasers based on net gain [40] as detailed below. First, an optical finite difference mode solver was used to calculate the transverse optical mode and effective mode index in the waveguide [41]. The refractive index of $Si_{0.07}Ge_{0.91}Sn_{0.02}$ lattice matched to Ge for barrier layers was extrapolated from [42] to be $n \approx 3.8$ at the GeCSn QW effective bandgap. Assuming isotropic material, the optical confinement factor, which measures the overlap of the optical mode with the cross-section area of the gain region, A, was then calculated using [43]:

$$\Gamma_{opt} = \frac{\iint_A \epsilon(\boldsymbol{r}) |E(\boldsymbol{r})|^2 d^2\boldsymbol{r}}{\iint_{-\infty}^{\infty} \epsilon(\boldsymbol{r}) |E(\boldsymbol{r})|^2 d^2\boldsymbol{r}}, \tag{1}$$

which sets the modal gain, $g\Gamma_{\mathrm{opt}}$, where g is the material gain per length in the QW. The subscript *opt* is used to distinguish the optical confinement factor from the Brillouin zone center, Γ. The permittivity, $\epsilon(\boldsymbol{r})$, may vary with position and material, especially if strains are nonuniform, but uniform materials are assumed here. All equations use SI units unless otherwise noted.

Threshold current density, J_{th}, is determined as follows. In a QW of thickness L_z,

$$J_{th} = \frac{qL_z}{\eta_i} \left\{ AN_{th}^2 + BN_{th}^2 + CN_{th}^3 \right\} \tag{2}$$

where η_{i} is injection efficiency (assumed to be 1), q is electron charge, N_{th} is the carrier density at threshold, A is the SRH coefficient, C is the Auger recombination coefficient (discussed later), and B is the bimolecular recombination coefficient [44]:

$$B = \frac{2(2\pi m_r k_B T)^{3/2}}{h^3 \tau_r N_C N_V}, \tag{3}$$

where k_{B} is Boltzmann's constant, h is Planck's constant, reduced mass $m_{\mathrm{r}} \equiv (m_{\mathrm{e}}{*}^{-1} + m_{\mathrm{hh}}{*}^{-1})^{-1}$ using density of states effective masses, N_{C} and N_{V} are the effective densities of states of the CB and VB, respectively, and the recombination lifetime τ_{r} of an electron-hole pair is

$$\tau_r^{-1} = \frac{4\pi n_r q^2 E_g}{3\epsilon_0 h^2 m_0^2 C_{op}^3} |M|^2, C_{op} \equiv \frac{\pi q^2}{n_{eff} c_0 \epsilon_0 m_0^2 \omega} \tag{4}$$

where E_{g} is bandgap, $\hbar\omega$ is photon energy, c_0 is the speed of light in vacuum, q is electron charge, ϵ_0 is the permittivity of free space, m_0 is electron rest mass, and n_{eff} is the refractive index or, in a waveguide, the effective index of the waveguide mode. Of these variables, only E_{g} varies significantly with strain and composition studied here. The momentum matrix element

$$|M|^2 = |\langle u_v | \hat{\boldsymbol{e}} \cdot \boldsymbol{p} | u_c \rangle|^2 \left(\text{in J . kg or} (mv)^2 \right) \tag{5}$$

is a material parameter: the fundamental strength of the optical transition [40], and part of the overall transition matrix element:

$$|M_T|^2 = |M|^2 |\langle \xi_v | \xi_c \rangle|^2 \tag{6}$$

where ξ_{v} and ξ_{v} be the envelopes of the respective wavefunctions. M is often assumed to equal the optical dipole matrix element times $im\omega$, but a correction factor is necessary in QWs or other finite volumes; TE mode lasing with heavy holes was assumed here [45], [46]. The wavefunction overlap integral, the second term in (6), accounts for selection rules and waveguide mode polarization, e.g., ∼1/2 for the TE mode with C-HH transitions for the lasers simulated here, with compressive strain (GeSn) or nearly lattice matched (GeC/GeCSn) [43]; Kane band theory [40] and density functional theory (DFT) [39] predict similar values for M across the materials studied here. Therefore, a value of $B = 10^{10} \mathrm{cm}^6 s^{-1}$ was used for all materials [23], and the remainder of this work focused on Γ_{opt}, N_{th}, and gain, as these all have stronger effects on J_{th}.

N_{th} is determined from net gain. Assuming a homogeneous gain region, the minimum gain to achieve laser threshold, g_{th}, is given when modal gain equals total modal loss:

$$\Gamma_{\mathrm{opt}}\, g_{th} = \langle \alpha_i \rangle + \alpha_m + \alpha_{FCA} \tag{7}$$

where $\langle \alpha_i \rangle$ is average internal loss, α_{m} is mirror loss, and α_{FCA} is free carrier absorption. We note in passing that spontaneous and amplified spontaneous emission (ASE) may both still be present in the spectrum at threshold, but threshold still provides a useful reference for comparing lasers. The material gain per unit length for a transition from a CB state to a VB state is [40]:

$$g(E_{cv}) = g_{\max}(E_{cv}) (f_c - f_v) \tag{8}$$

Neglecting excitons and line shape broadening, the maximum possible gain (or absorption) is

$$g_{\max}(E_{cv}) = \frac{\pi q^2 h}{n_{eff} \epsilon_0 c_0 m_0^2} \frac{1}{\hbar \omega_{cv}} |M_T(E_{cv})|^2 \rho_r(E_{cv}) \tag{9}$$

where ρ_{r} is the reduced or joint density of states, and k_{B} is the Boltzmann constant. f_{c} and f_{v} are the Fermi-Dirac occupation

Authorized licensed use limited to: Texas State University. Downloaded on May 19,2025 at 15:53:30 UTC from IEEE Xplore. Restrictions apply.

factors for carrier populations n or p, respectively, from quasi-Fermi levels E_{Fn} and E_{Fp}:

$$f_c(E) = \frac{2}{\sqrt{\pi}(k_B T)^{3/2}} \int_{E_c}^{\infty} \frac{\sqrt{E}}{\exp\left(\frac{E-E_{Fn}}{k_B T}\right)+1} dE, \quad (10a)$$

$$f_v(E) = \frac{2}{\sqrt{\pi}(k_B T)^{3/2}} \int_{E_v}^{-\infty} \frac{\sqrt{E}}{\exp\left(\frac{E-E_{Fp}}{k_B T}\right)+1} dE, \quad (10b)$$

For a QW, this reduces to, for electrons and holes, respectively:

$$f_c,\ f_v = \ln\left[1+\exp\left(\frac{E_{Fn,p}-E_n}{k_B T}\right)\right], \quad (11)$$

where E_n is the energy of the nth QW state, with n = 1 for the fundamental or lasing transition, and energy is defined positive upwards for holes. For bulk materials (for example, bulk heterojunction lasers) and QWs, respectively, assuming parabolic bands [23], [43]:

$$\rho_{r,3D}(\hbar\omega - E_{G,eff}) = \frac{(2m_r)^{3/2}}{2\pi^2\hbar^2}\sqrt{\hbar\omega - E_{G,eff}} \quad (12)$$

$$\rho_{r,2D} = \frac{m_r}{\pi\hbar^2 L_z} \text{ per QW state} \quad (13)$$

where $E_{G,eff}$ is the effective bandgap, which includes material bandgap plus electron and hole confinement energies [47]. Consequently, the electron concentration N_s in a given state s, whether 3D bulk CB or 2D QW, at energy E_s with effective mass m_s, is given by

$$N_s = \int_{E_s}^{\infty} f(E)\,\rho(E)\,dE \quad (14)$$

$$N_{s,3D} = \frac{m_s^{*3/2}}{3\sqrt{2}\pi^2} \int_{E_s}^{\infty} \frac{\sqrt{E-E_s}}{\exp\left(\frac{E-E_{Fn}}{k_B T}\right)+1} dE, \text{ or} \quad (15)$$

$$N_{s,2D} = \frac{m_s^* k_B T}{\pi\hbar^2 L_z} \ln\left[1+\exp\left(\frac{E_{Fn}-E_s}{k_B T}\right)\right] \quad (16)$$

and similarly for holes. Threshold occurs when $f_c - f_v$ is sufficient to overcome losses, and E_{Fn} and E_{Fp} can then be determined by substituting (15) or (16) into (2) and solving numerically [48].

Because the Ge valence band is not significantly modified by GeC or GeSn except through strain, valence inter-subband absorption and Auger coefficients were assumed to be the same across materials studied here, with the same dependence on wavelength, unless otherwise noted. Temperature effects on the band structure itself were also neglected here, as the directness (E_L - E_Γ separation) is a weak function of temperature compared with the relative thermal occupations of these CB valleys.

Representative $Ge_{1-x}Sn_x$ material data were taken from [23], [30], including band offsets, deformation potentials, and masses of the CB constant-energy ellipsoids for the L and Γ valleys. (See Table I and Supplemental Materials.) These data appear to slightly underestimate the fraction of Sn required for a given amount of directness compared with experimental reports, so the GeSn results reported below are likely optimistic compared with experiment. Lattice constants were calculated using Vegard's Law starting from Si (0.543Å), Sn (0.646Å), Ge (0.566Å), C (0.3567Å). In strained Ge, the Ge CB effective mass was calculated from its bandgap using the 4-band Kane model.

TABLE I
MATERIAL PARAMETERS USED FOR SiGeSn [23], [30]

$m_{L,par}(Sn)/m_0 = -0.1770\ Sn^2 + 0.2759\ Sn + 1.6742$
$m_{L,perp}(Sn)/m_0 = 0.0266\ Sn^2 - 0.0447\ Sn + 0.0914$
$m_{e\Gamma}(Sn)/m_0 = 0.0104\ Sn^2 - 0.1308\ Sn + 0.0416$ (isotropic)
[A] $m_{HH}/m_0 = 0.33$
[B] $m_{LH}(Sn)/m_0 = 0.0067\ Sn^2 - 0.1684\ Sn + 0.0519$
$m_{SOH}(Sn)/m_0 = -0.2079\ Sn + 0.1271$ [49]
$m_{DOS}/m_0 = (4^2 m_l m_t^2)^{1/3}$
$m_{cond}/m_0 = 3\ m_l m_t (2m_l + m_t)^{-1}$
$E_{\Gamma,SiGeSn}(Si, Sn)/eV = (1 - Sn - Si)\cdot 0.80 - 0.41\ Sn + 4.06\ Si - 1.94\ Sn\ (1 - Sn - Si) - 0.21\ Si\ (1 - Sn - Si) + 13.2\ Si\ Sn$
$E_{LSiGeSn}(Si, Sn)/eV = (1 - Sn - Si)\cdot 0.67 + 0.14\ Sn + 2.0\ Si + 0.11\ Sn\ (1 - Sn - Si)$
$E_{VBav}(Si, Sn)/eV = -0.48\ Si + 0.69\ Sn$
$d_{ESO}(Si, Sn)/eV = 0.295\ (1 - Sn - Si) + 0.800\ Sn + 0.043\ Si$
$E_{VM}(Si, Sn)/eV = E_{VBav}(Si, Sn) + (1/3)\ d_{ESO}(Si, Sn)$
$E_{CM\Gamma}(Si, Sn)/eV = E_{VM}(Si, Sn) + E_{\Gamma SiGeSn}(Si, Sn)$
$E_{CML}(Si, Sn)/eV = E_{VM}(Si, Sn) + E_{LSiGeSn}(Si, Sn)$
$E^h_{d,\Gamma} = \partial E_\Gamma/\partial\epsilon_{xx} = -0.099$ eV/%strain [30]
$E^h_{d,L} = \partial E_L/\partial\epsilon_{xx} = -0.020$ eV/%strain [30]

[A] Assumed unchanged with Sn or strain.
[B] Nearly isotropic; value along (100) direction was used.

TABLE II
MATERIAL PARAMETERS FOR GeCSn FROM VASP

$m_\Gamma/m_0 = 0.072$ (isotropic)
$m_{L,DOS}$ and $m_{L,cond}$: same as Table I
$E_{g\Gamma}/eV = E_{c\Gamma} - E_{v.} = 0.446$
$E^h_{d,\Gamma} \equiv \partial E_{g\Gamma}/\partial\epsilon_{xx} = -0.129$ eV/%strain
$E_{gL}/eV = E_{cL} - E_v = 0.670$
$E^h_{d,L} \equiv \partial E_{gL}\ \partial\epsilon_{xx} = -0.112$ eV/%strain

Because the experimental properties of GeCSn are still uncertain, unless otherwise specified below, these were generated using the Vienna Ab-initio Simulation Package, (VASP) following techniques in [39] and shown in Table II.

It is a common error to use the same value of electron effective mass for both quantum confinement and population, but these differ for anisotropic valleys. For the CB L valley, including the 4-fold degeneracy, the density of states (DOS) effective mass is $m*_{DOS} = (4^2 m_l m_t^2)^{1/3}\ m_0$, where m_l and m_t are the longitudinal and transverse masses of the constant energy ellipsoid, respectively. QW confinement energies must be calculated using the conductivity effective mass of a single valley, which is, for the (100) QWs modeled in this work,

$$m^*_{cond} = 3\left(m_l^{-1} + 2m_t^{-1}\right)^{-1} \quad (17)$$

(see Supplemental Material) [50]. For example, in $Ge_{0.83}Sn_{0.17}$, $m*_{DOS,L} = 0.58\ m_0$, while $m*_{cond,L} = 0.12\ m_0$. Similarly, populations of the valence bands must be determined from $m*_{DOS,HH}$ and $m*_{DOS,LH}$ weighted by their relative energies, which differ if the layer is biaxially strained.

Authorized licensed use limited to: Texas State University. Downloaded on May 19,2025 at 15:53:30 UTC from IEEE Xplore. Restrictions apply.

Lasing is driven by electrons in the lowest confined Γ QW state, Γ_1. In turn, the fraction of electrons, $F_{\Gamma 1}$, in Γ_1 is given by the ratio of population of that state to all QW states, considering only confined electrons:

$$F_{\Gamma 1} = \frac{n_{\Gamma 1,2D}\left(E_{\Gamma 1}, E_{Fn}, m^*_{e\Gamma}\right)}{\sum_i n_{i,2D}\left(E_i, E_{Fn}, m^*_i\right)} \tag{18}$$

where *i* indexes all states in the QW, both direct and indirect.

The transparency condition provides an initial estimate for quasi-Fermi levels (QFLs). Whether in bulk material or a QW, transparency occurs when the QFLs are separated by an energy equal to the bandgap [51] or, for a QW, the effective bandgap between the lowest confined electron and hole states (E_{e1} and E_{h1}, respectively):

$$\left(E_{\mathrm{Fn}} - E_{\mathrm{Fp}}\right)|_{\mathrm{transp}} = E_{\mathrm{G}} + E_{e1} + E_{h1} \tag{19}$$

This gives a lower limit for the separation of quasi-Fermi levels: the threshold in an infinitely long, lossless laser. Mirror and other losses in an actual laser will require additional gain to compensate, requiring even greater separation between QFLs. Because the effective masses of electrons and holes are often different (for example, $m*_{HH}/m*_{e\Gamma} \approx 8$ for Ge), the CB is usually degenerate, with E_{Fn} above the CB minimum (CBM). E_{Fn} and the corresponding electron concentration, N_{tr}, at transparency can be found by solving $n_\Gamma(E_{Fn}) = p_\Gamma(E_{Fp})$ subject to (19). For example, using the ratio of effective masses for Ge given above, at transparency, E_{Fn} in an arbitrary QW will be 38 meV above the lowest confined state at 27 °C, and 33 meV at 100 °C. E_{Fn} is even higher in GeSn, due to its smaller $m^*_{e\Gamma}$.

For the analysis below, hole masses from bulk GeSn were used, and heavy (light) holes were assumed to dominate in compressive (tensile) strained layers. Other VB effects such as quantized hole levels or small changes in band curvature due to strain [31], [32] were not considered here, as this work focused on the CB, where the effects of C and Sn are most pronounced. Strain is expected to have similar, predictable effects on all the materials studied here [52], allowing direct comparisons. Also, because the fraction of Sn in GeCSn is small, while the CB offset from GeC or GeCSn to Ge is large, similar conclusions will apply to GeC and GeCSn unless otherwise noted below (e.g., strain), though GeCSn is easier to grow [34].

III. Results and Discussion

A. Directness: Confinement in K-Space

The first requirement for low-threshold lasers is a direct bandgap: confinement in *k*-space. Electrons in indirect L CB valleys contribute no gain [43] but instead reduce differential gain $\partial g/\partial n$, because extra electrons must be injected to fill the L states as well as Γ states. This also increases FCA and Auger losses because more holes are needed to maintain charge neutrality, as discussed later [23]. Use of L valleys as a reservoir for Γ electrons appears to be unnecessary since the stimulated radiative lifetime is comparable with the energy relaxation time and intervalley scattering time, both of which are on the order of ~0.2 ps with or without strain [54], [55], [56]. In other words, the bottom of the CB Γ valley will remain populated regardless of which valley is being pumped, so spectral hole burning is unlikely. Adding Sn or strain decreases the effective mass, $m*_{e\Gamma}$, which partly depopulates the Γ valley (i.e., fewer electrons for the same amount of directness), as does increasing temperature, shown in Fig. 1. Directness in Fig. 1(x axis) might be achieved by tensile strain and/or composition. The labeled GeSn compositions assume fully relaxed GeSn; any residual compressive strain would reduce directness. Ge with 2.8% tensile strain for 90 meV of directness [27] is only somewhat better: 25% of electrons in the direct Γ valley at room temperature, falling to 16% at 100 °C.

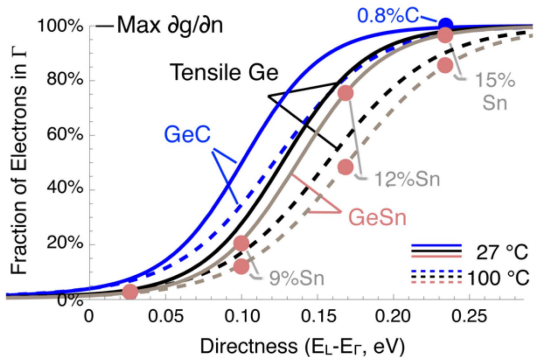

Fig. 1. GeC(Sn) confines electrons in the lasing Γ_1 state better than tensile Ge or relaxed GeSn for the same directness. Differential gain $\partial g/\partial n$ is maximized when all electrons are in Γ_1. GeSn and t-Ge slopes are shallower than GeC due to progressively lighter effective mass with added Sn or strain. After [53], parts ©2023 IEEE.

Furthermore, a *strongly* direct gap is necessary because the L valley density of states effective mass ($m*_{L,DOS} \approx 0.6\ m_0$) is more than 30 times larger than that of the Γ valley ($m*_{\Gamma,DOS} < 0.02\ m_0$ for 17%Sn) [23], [30]. Even if 100 meV of directness was achieved, i.e., the direct Γ valley 100 meV below the indirect L valley [57], at room temperature, *half* of the electrons are still in the indirect L valley since the population ratio is proportional to $(m*_1/m*_2)^{3/2}$. Achieving even this amount of directness is unlikely for lasers using tensile strain alone in pure Ge due to the fragility of tensile Ge under the extreme strains required, leading to dark line defects propagating in real time when perturbed [58]. On the other hand, $Ge_{1-x}C_x$ (GeC) with <1%C has $m*_{e\Gamma} \approx 0.05$-$0.08\ m_0$ according to ab-initio calculations [59], so most of the electrons are in the Γ valley even for temperatures above 100 °C and modest directness.

Strain is another issue for GeSn lasers. The compressive strain from adding Sn nearly doubles the amount of Sn required to achieve a given directness [60]. GeSn/Ge QWs thin enough to have a single confined state in Γ (width $w \sim 15$ nm) have only 32 meV of directness, which is less than kT at 100 °C, and they lose it entirely when $w \leq 10$ nm, according to finite well [23], [30], [43] and pseudopotential calculations [61]. The unwanted compressive strain can be reduced by growing low-Sn GeSn on relaxed, high-Sn GeSn buffer layers, and this approach has enabled electrically pumped lasers up to 100K [17], [18], [62]. Fig. 2 shows the directness of unconfined bulk $Ge_{1-x}Sn_x$ grown on a fully relaxed $Ge_{1-b}Sn_b$ buffer layer. However, to

Authorized licensed use limited to: Texas State University. Downloaded on May 19,2025 at 15:53:30 UTC from IEEE Xplore. Restrictions apply.

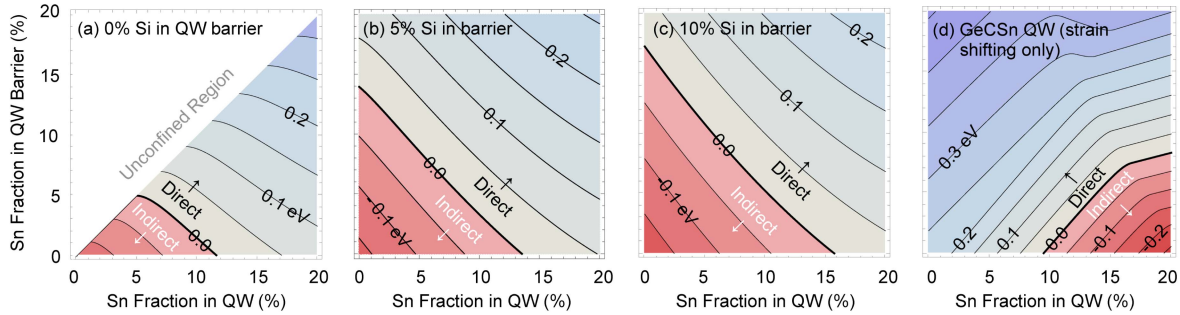

Fig. 2. Directness (E_L - E_Γ, in eV) for 12 nm wide QWs, coherently strained to fully relaxed SiGeSn barriers: (a)-(c) $Ge_{1-x}Sn_x$ in $Si_aGe_{1-a-b}Sn_b$ varying Si, and (d) $Ge_{0.992-x}C_{0.008}Sn_x$ in $Ge_{1-b}Sn_b$ including only shifts of GeC directness due to strain from adding Sn to QW and barrier; actual directness may vary with C-Sn arrangement. Adding Si to barriers reduces directness by reducing the lattice constant, increasing compressive strain in QW, but adding 0.8%C restores strongly direct character except under high compressive strains.

compensate for the reduced bandgap in the high-Sn barriers, relatively high concentrations of Si must be added to create SiGeSn QW barriers. As we shall see later, this greatly degrades optical confinement and modal gain. On the other hand, for GeCSn on Ge, each 1% of carbon (small atom) compensates the strain of 4.6% of Sn (large atom), greatly reducing the unwanted effects of compressive strain.

B. Band Offsets: Real Space Confinement

A strongly direct gap is necessary but not sufficient for lasing even at room temperature. Room temperature lasing in early GaAs lasers was only achieved when heterojunctions were added for physical confinement of carriers in a QW (or QD) [63], which is thus a second requirement for low-threshold lasers. QWs dramatically reduce laser thresholds because quantum confinement induces a 2D density of states, which increases carrier populations at the effective band edges [64]. QWs also force electrons and holes into the same physical space, further increasing gain due to the increased overlap between their wavefunctions [65]. QWs may also increase the optical dipole matrix element by 1.5x for TE modes [66]. For maximum gain, the QW should be narrow enough that only a single state is populated, so more electrons contribute to gain (Fig. 4), with less thermal broadening of population [40], [67]. In III-V lasers, this was addressed using narrower QWs or QDs, which enabled nearly thresholdless lasing [68], [69], [70], [71], [72], and lasing above 200 °C [73].

However, such confinement is impractical for most Group IV lasers since no composition of GeSn or tensile Ge retains a direct bandgap in a QD or narrow QW [74]. Quantum confinement raises the energies of QW states as roughly the inverse of their effective masses (1/m∗∗). Therefore, the light mass Γ valley in GeSn and t-Ge is pushed up much faster with confinement than the heavy, indirect L valley, and the direct bandgap is degraded or lost. GeSn suffers particularly since $m*_{e\Gamma}$ is 2-4 times lighter than in Ge [47]. However, t-Ge is limited by its critical thickness, which allows a maximum QW width of just 4 nm [75] for the case of 2.8% tensile strain mentioned above. As with GeSn, the Γ valley is pushed above the L valley, and the t-Ge QW becomes indirect again.

In contrast, GeC(Sn) QWs not only start deeper, but they also have an electron effective mass $m*_{e\Gamma}$ that is 2-5x larger than GeSn, preserving a single, strongly direct CB state even in a narrow QW (Fig. 3). The heavy electron effective mass is a hallmark of band anticrossing in highly mismatched alloys [76]. This increases differential gain because electrons are not wasted in higher energy states.

Fig. 4 shows the energies and relative occupations of each CB QW state as a function of QW width. For GeSn QWs in SiGeSn barriers, the maximum fraction of electrons in Γ_1 is 62%, obtained at a QW width of 16 nm at 27 °C. At higher temperatures, electrons populate higher energy states, so the relative occupation of Γ_1 drops (red arrow) to 40% at 100 °C. In contrast, for GeC QWs in Ge barriers, even narrow, 5-10 nm QWs have nearly 100% occupation in the Γ_1 state, as highlighted by the blue arrow, and this high occupation is almost unchanged at 100 °C.

Deep QWs also reduce loss from thermal escape of carriers to further reduce thresholds. For example, even in InGaAsP, which has the desirable, heavier electron effective masses, an extra 0.3 eV barrier still reduced leakage currents by 33x [43]. Thus, strong confinement by a *deep* QW is crucial at CPU temperatures [43], [77], [78]. For GeSn QWs, using SiGeSn instead of Ge for the barriers could provide confinement up to ∼200 meV for 10% Si [61], [74], [79], [80], [81], but at the cost of optical confinement (see below). In contrast, GeCSn QWs are both deeper and have larger $m_e^* = 0.05\ m_0$ to $0.08\ m_0$, reducing thermal leakage currents.

C. Optical Confinement

Finally, optical confinement maximizes the optical mode within the QW for maximum gain [82]. Here GeC(Sn) offers a significant advantage over carbon-free GeSn. Since Si (as SiGeSn) is not necessary for carrier confinement, it is available for optical cladding layers with low refractive index, i.e., separate confinement heterostructures (SCH, Fig. 5) [83], [84], [85], [86].

In contrast, GeSn QWs without C typically require relaxed, high-Sn buffer layers to reduce strain [87], [88], [89], but this produces claddings with *higher* refractive index, pulling the

Authorized licensed use limited to: Texas State University. Downloaded on May 19,2025 at 15:53:30 UTC from IEEE Xplore. Restrictions apply.

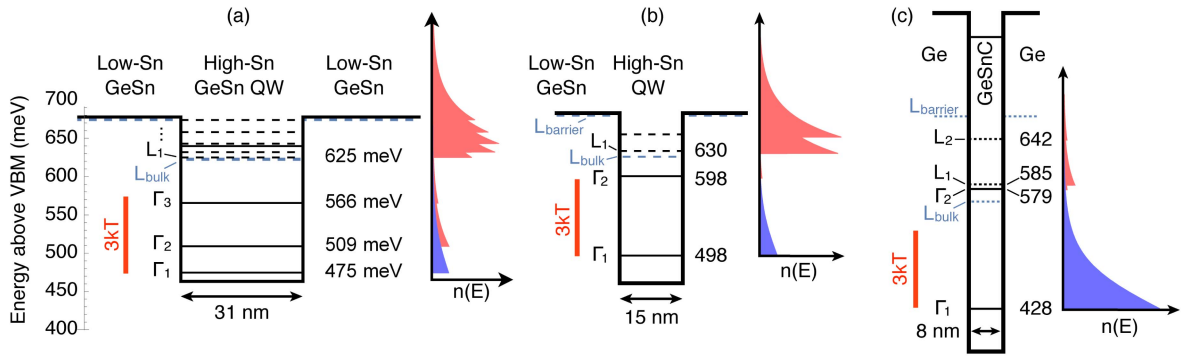

Fig. 3. Energies of confined CB states and corresponding electron distributions at 100 °C for (a) 31 nm GeSn QW in SiGeSn barriers, (b) 15 nm GeSn QW in SiGeSn barriers, and (c) 8 nm GeC QW in Ge barriers. Relative population in the lasing state (Γ_1) is shown in blue; all others in red. Bulk L valley CBM is dashed green; QW L states are dashed black. L1 in (e) is unconfined. Red bar shows 3kT at 100 °C. After [53], parts ©2023 IEEE.

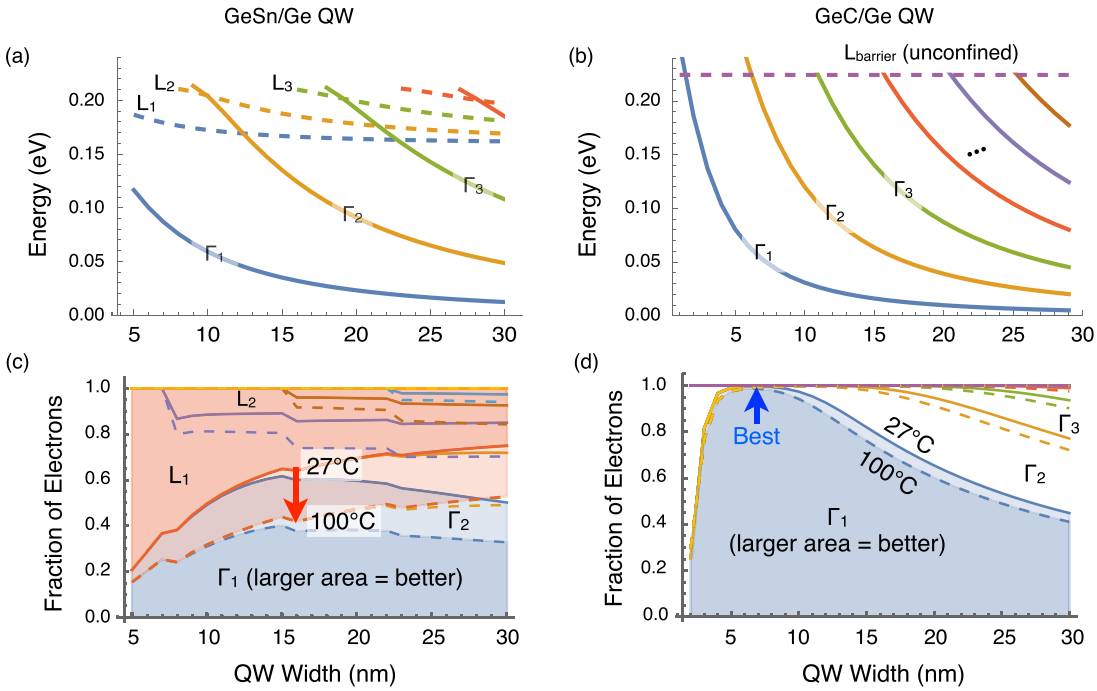

Fig. 4. (a)-(b): Energies of confined CB states for (a) GeSn QW in SiGeSn barriers, and (b) GeC QW in Ge barriers, as a function of QW width. (c)-(d): Fraction of electrons in each QW state for (a) and (b), respectively, after [53], ©2023 IEEE. Blue regions represent fraction of electrons in Γ_1 state; pink is fraction in L states. Solid lines are boundaries of occupation of each state at 27 °C; dashed lines: at 100 °C. Maximum differential gain $\partial g/\partial n$ when 100% of electrons are in Γ_1 state.

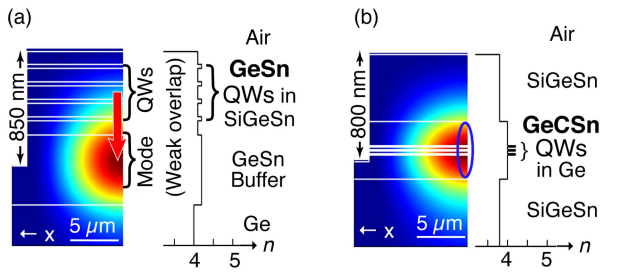

Fig. 5. Laser mode and refractive index n profiles for: (a) GeSn/SiGeSn (recalculated from Margetis) and (b) GeCSn/Ge QW with SiGeSn optical cladding layers. Red arrow highlights pulling of optical mode away from QWs by high-index buffer layer. GeCSn keeps optical mode centered at QWs (blue circle). After [53], parts ©2023 IEEE.

optical mode away from the QWs (Fig. 5(a)) [90]. Even for very wide 31 nm GeSn QWs, which only have 25% of electrons in the lowest Γ state at 300K (Fig. 4), the total optical confinement factor was reported as only 7.3% over four QWs, ranging from 0.3% for the top QW to 3.48% for the QW closest to the centroid of the mode [90]. Reducing the Si content to improve the optical confinement factor [57] results in loss of carrier confinement, limiting lasing to cryogenic temperatures. In contrast, by keeping the mode centered at the QWs, GeCSn provides the same optical confinement factor with a quarter of the gain volume: four 8 nm QWs in 10 nm Ge barriers, Fig. 5(b) [41]. Furthermore, GeCSn has lower strain than GeSn, allowing growth of additional QWs without exceeding the critical thickness [31].

Authorized licensed use limited to: Texas State University. Downloaded on May 19,2025 at 15:53:30 UTC from IEEE Xplore. Restrictions apply.

The freedom in choice of strain in GeCSn may also help avoid the Type II valence band alignment reported for GeSn/SiGeSn QWs [57].

It is worth noting that careful selection of doping can slightly reduce the threshold in GeSn lasers, but reported predictions for threshold were still above 1.2 kA/cm^2 [23], [30]. Doping is expected to produce similar slight improvement in GeC(Sn) lasers, so the present work focuses instead on gain and confinement.

D. Auger Recombination

In addition to the confinement requirements for gain listed above, high temperature laser designs must also minimize losses. These may be generally divided into Auger recombination [91] and free carrier absorption (FCA), which includes both plasma absorption (Drude model) [23] and inter-valence band absorption (IVBA) [92]. FCA is the dominant loss in existing Ge-based lasers such as GeSn [12], [29], [61], [91], but both IVBA and Drude absorption increase with wavelength. Because FCA increases proportionally with carrier density [93], and Auger recombination by its cube, even small reductions in threshold have an outsized effect in reducing losses. We consider contributions from each of these losses separately below.

Auger coefficients may themselves be dependent upon carrier density, and also may increase by orders of magnitude with just 0.37% tensile strain [94]. However, adding even a few percent of Sn may reduce Auger losses by even more than this, partially by increasing the split-off energy [95]. GeC induces only weak tensile strain due to the very small fraction of C in the alloy, and almost no change in the VB, so hole-dominated Auger processes such as CHHS and CHHL are expected to be similar to Ge. Despite the reduced bandgaps, which tend to increase Auger recombination, the lack of directly comparable data for each material led to use of Auger coefficients here for Ge for both GeSn (as in [23]) as well as GeCSn. Similarly, the effects of Sn on the VB, and therefore CHHS/CHHL Auger recombination, are expected to be very similar for GeSn vs. GeCSn, allowing relative comparisons. Adding C to GeSn may provide the gain and confinement advantages presented in this work while taking advantage of the decrease in Auger recombination.

To illustrate the effect that a larger Auger coefficient would have, thresholds were also calculated using C = 3.2 × 10^{-28} cm^6 s^{-1} in (2) from a direct bandgap material (InGaAs) [96] with a similar bandgap, instead of that of Ge. This increased all calculated threshold current densities accordingly. Using this new C, at 100 °C, the threshold for a 5 QW GeCSn laser increased ~7× from 0.16 kA cm^{-2} to 1.2 kA cm^{-2}, while a carbon-free GeSn laser increased even more sharply, from 14 kA cm^{-2} to 132 kA cm^{-2} (9×). These results further emphasize the benefit of adding carbon to GeSn. However, they should be considered qualitative, as detailed calculations of the Auger coefficient [96] are beyond the scope of this paper.

E. Free Carrier Absorption

Plasma absorption may occur for heavy and light holes, as well as electrons in the CB L and Γ valleys. A Drude model was used to estimate plasma FCA from all four of these states [23]. Due to a lack of GeSn data on free carrier mobilities and their dependence on concentration and temperature, following, the carrier-averaged expressions from [31] were used, except the proportionality relation $\mu_{e\Gamma}$, / $\mu_{eL} \approx m_{eL}$ / $m_{e\Gamma}$ was used because drift mobility is inversely proportional to effective mass according to the Einstein relation. Also, to handle heavy holes (HH) and light holes (LH) separately, as a first order correction, the respective mobilities μ_{hh} and μ_{lh} were estimated using their effective masses and a conductivity sum rule. It can be shown (see Supplementary Information) that the HH and LH mobilities (μ_{HH}, μ_{LH}) can be approximated as functions of the average hole mobility, $\mu_{h,avg}$, which is a function of hole concentration and temperature:

$$\mu_{HH}\left(n_{HH},T\right) \approx \frac{m_{HH}^{3/2}+m_{LH}^{3/2}}{m_{HH}^{3/2}+m_{HH}m_{LH}^{1/2}}\mu_{h,avg}\left(p_{HH},T\right) \tag{20}$$

$$\mu_{LH}\left(n_{LH},T\right) \approx \frac{m_{HH}^{3/2}+m_{LH}^{3/2}}{m_{LH}^{3/2}+m_{LH}m_{HH}^{1/2}}\mu_{h,avg}\left(p_{LH},T\right) \tag{21}$$

where n_{hh} and n_{ln} are the concentrations of heavy and light holes, respectively, and T is temperature. Using these mobilities, the Drude model predicts an absorption coefficient for any particular state (LH, HH, CB) as follows:

$$\alpha_{Drude(\lambda,n_{conc})} = \frac{10^{-4}q_0^3\lambda^2 n_{conc}}{4\pi^2 {c_0}^3 n_r \epsilon_0 {m_h^*}^2 \mu} \tag{22}$$

in cm^{-1}, where λ is wavelength of incoming light in μm, n_{conc} is concentration of carriers in the state in cm^{-3}, μ is mobility in cm^{2}V^{-1}s^{-1}, m^* is conductivity effective mass of the state. Alloy scattering in both GeSn and GeC(Sn) will reduce all free carrier mobilities from the values used here, particularly at low temperature, but this does not significantly change the comparisons presented below.

FCA can also be caused by intervalence band absorption (IVBA), particularly from light or heavy holes to the split-off band. This transition is forbidden at $k = 0$ but increases rapidly as k^2 [97]. This leads to a rapidly increasing joint density of states for the absorption proportional to $(h\nu - E_G)^{3/2}$.

In principle, Sn could eliminate IVBA by increasing the spin-orbit (SO) splitting of the VB. If the spin-orbit splitting, $E_{HH/LH} - E_{SOH}$, is larger than the effective bandgap, then intervalence band absorption (IVBA) is essentially eliminated within the gain region. For example, $Ge_{0.85}Sn_{0.15}$ has a bandgap of roughly 0.34 eV and a spin-orbit splitting of 0.36 eV. Even when pumped to transparency, the IVBA near the band edge would be negligible, at least in bulk material. Furthermore, compressive strain pushes the light hole band with its large IVBA farther away from the quasi-Fermi level, reducing the number of light holes and corresponding LH-SO absorption.

However, that same compressive strain also increases the effective bandgap, as does QW confinement. This leads to sharply increased IVBA. Thus, IVBA seems likely to remain a dominant source of loss in practical GeSn lasers. Furthermore, IVBA may still exist in the barrier layers, where the Sn concentration is lower and spin-orbit splitting is smaller. On the other hand, the

Authorized licensed use limited to: Texas State University. Downloaded on May 19,2025 at 15:53:30 UTC from IEEE Xplore. Restrictions apply.

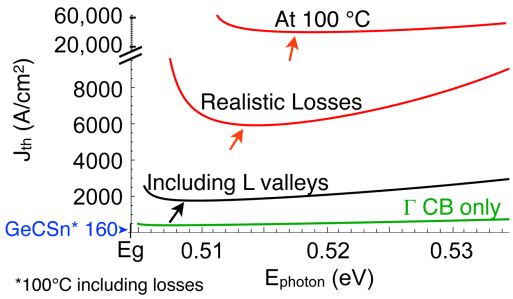

Fig. 6. Calculated $Ge_{0.9}Sn_{0.1}$ DH laser threshold current density J_{th} vs. photon energy E_{photon}. Green: All injected electrons forced to Γ CB valley and assuming no losses. Black: CB L valleys allowed to populate, but still lossless. Red: Adding realistic losses first, then high temperature. Blue: Calculated threshold of GeCSn MQW laser at 100 °C including same losses. After [53], parts ©2023 IEEE.

low thresholds in GeC(Sn) lasers reduce IVBA by reducing the free hole concentration. Precise calculations of IVBA require exact solutions to wave functions including band anisotropy, so IVBA was therefore omitted from FCA calculations presented here. Detailed calculations are underway and will be presented elsewhere.

F. Other Nonradiative Recombination

Other nonradiative recombination such as Shockley-Reed-Hall (SRH) was neglected for this analysis, as it primarily originates from technological parameters such as the quality of material growth and surface passivation. This assumes comparable material quality is possible as growth of each material matures.

G. Effects on Laser Thresholds

To illustrate the effect of the above conditions on laser performance, the threshold current density for $Ge_{0.86}Sn_{0.14}$ / $Si_{0.03}Ge_{0.89}Sn_{0.08}$ DH lasers was calculated under various conditions, along with $Ge_{98.44}C_{0.78}Sn_{0.78}$ QW lasers at 100 °C, all assuming broad area edge emitting lasers with cleaved end facets. Unless otherwise noted as lossless, all lasers included FCA and Auger recombination, injection efficiency of 80%, and a cavity length of 1 mm. The GeCSn lasers used five 10nm-thick QWs with Ge barriers and SiGeSn optical cladding layers, an optical overlap of 7% per QW calculated as in Fig. 5, and an injection efficiency of 100% due to the high QW barriers plus SCH for further carrier confinement.

Even though the GeSn L CB valley was 0.12 eV higher than the Γ valley, with only 45% of injected electrons in the higher L valley, the reduction in differential gain led to a 3.3x increase in threshold current from 459 to 1520 A $cm^{7minus;2}$ even in lossless lasers, as shown in Fig. 6. Adding realistic losses such as FCA, 40% injection efficiency (est. from [22]), and a reduced optical overlap of 75% further increased the detrimental effect of the L valleys since more gain was required to overcome these additional losses, but instead the differential gain was reduced. High temperatures further compounded these effects, leading to J_{th} above 39 kA cm^{-2} at 100 °C.

IV. Conclusion

The progress of GeSn lasers toward electrically pumped operation at room temperature or higher is limited by weak confinement of both electrons and photons. Even assuming ideal material growth, predicted threshold current densities for GeSn/SiGeSn lasers on a 100 °C process core approach 40 kA·cm^{-2}. Providing the necessary additional confinement is a significant challenge due to the small CB offsets at heterojunctions, lack of a suitable low-index cladding layer, and weak directness. The very light electron effective mass in GeSn means many electrons remain in the indirect L valley, especially when confined in a narrow QW, contributing to free carrier losses rather than gain. On the other hand, strong confinement of both electrons and photons is predicted with the addition of a few percent of carbon to Ge or GeSn, forming GeC(Sn), because the highly mismatched but isovalent Group IV carbon atoms shift the direct CB valley well below the indirect valley. This leads to a marked reduction in threshold current density. The reduction in threshold is further magnified by the reduced free carrier losses, which further reduced predicted thresholds in GeCSn MQW lasers as low as 160 A·cm^{-2} even at 100 °C. These results are highly promising for dilute germanium carbide GeC(Sn) lasers that can be integrated directly within hot processor cores.

Acknowledgment

The authors thank Mark Holtz for helpful discussions and Mohammed Reaz Rahman Munna for editing assistance.

References

[1] S. K. Moore, "Cerebras' new monster AI chip adds 1.4 trillion transistors," *IEEE Spectr.*, vol. 20, Apr. 2021. [Online]. Available: https://spectrum.ieee.org/cerebras-giant-ai-chip-now-has-a-trillions-more-transistors

[2] T. Bang, N. May, I. Petrov, and C. Binnig, "The full story of 1000 cores: An examination of concurrency control on real(ly) large multi-socket hardware," *Very Large Data Bases J.*, vol. 31, no. 6, pp. 1185–1213, 2022, doi: 10.1007/s00778-022-00742-4.

[3] D. A. B. Miller, "Rationale and challenges for optical interconnects to electronic chips," *Proc. IEEE*, vol. 88, no. 6, pp. 728–749, Jun. 2000.

[4] M. Miscuglio and V. J. Sorger, "Photonic tensor cores for machine learning," *Appl. Phys. Rev.*, vol. 7, no. 3, 2020, Art. no. 031404.

[5] B. J. Shastri et al., "Photonics for artificial intelligence and neuromorphic computing," *Nat. Photon.*, vol. 15, no. 2, pp. 102–114, 2021.

[6] V. Sze, Y.-H. Chen, T.-J. Yang, and J. S. Emer, "Efficient processing of deep neural networks: A tutorial and survey," *Proc. IEEE*, vol. 105, no. 12, pp. 2295–2329, Dec. 2017.

[7] M. Al-Qadasi, L. Chrostowski, B. Shastri, and S. Shekhar, "Scaling up silicon photonic-based accelerators: Challenges and opportunities," *APL Photon.*, vol. 7, no. 2, 2022, Art. no. 020902.

[8] J. E. Bowers, "Laser integration on silicon for photonic integrated circuits," *Proc. SPIE*, vol. PC12004, 2022, Art. no. PC1200402.

[9] S. Bubeck and M. Sellke, "A universal law of robustness via isoperimetry," in *Proc. Adv. Neural Inf. Process. Syst.*, 2021, vol. 34, pp. 28811–28822.

[10] D. Q. Kelly, I. Wiedmann, D. I. Garcia-Gutierrez, M. Jose-Yacaman, and S. K. Banerjee, "Thin germanium-carbon layers on silicon for MOS applications," *ECS Trans.*, vol. 3, no. 7, 2006, Art. no. 1077, doi: 10.1149/1.2355902.

[11] M. A. Wistey, Y. Y. Fang, J. Tolle, A. G. Chizmeshya, and J. Kouvetakis, "Chemical routes to Ge/Si(100) structures for low temperature Si-based semiconductor applications," *Appl. Phys. Lett.*, vol. 90, no. 8, Feb. 2007, Art. no. 082108, doi: 10.1063/1.2437098.

[12] Q. M. Thai et al., "GeSn optical gain and lasing characteristics modelling," *Phys. Rev. B*, vol. 102, no. 15, 2020, Art. no. 155203.

Authorized licensed use limited to: Texas State University. Downloaded on May 19,2025 at 15:53:30 UTC from IEEE Xplore. Restrictions apply.

[13] R. E. Camacho-Aguilera et al., "An electrically pumped germanium laser," *Opt. Exp.*, vol. 20, no. 10, pp. 11316–11320, 2012, doi: 10.1364/OE.20.011316.

[14] A. Elbaz et al., "Ultra-low-threshold continuous-wave and pulsed lasing in tensile-strained GeSn alloys," *Nat. Photon.*, vol. 14, no. 6, pp. 375–382, 2020, doi: 10.1038/s41566-020-0601-5.

[15] S. Wirths et al., "Lasing in direct-bandgap GeSn alloy grown on Si," *Nat. Photon.*, vol. 9, no. 2, pp. 88–92, 2015, doi: 10.1038/nphoton.2014.321.

[16] V. Reboud et al., "Optically pumped GeSn micro-disks with 16% Sn lasing at 3.1 μm up to 180 K," *Appl. Phys. Lett.*, vol. 111, no. 9, 2017, Art. no. 092101, doi: 10.1063/1.5000353.

[17] D. Stange et al., "Optically pumped GeSn microdisk lasers on Si," *ACS Photon.*, vol. 3, no. 7, pp. 1279–1285, Jul. 2016, doi: 10.1021/acsphotonics.6b00258.

[18] S. Al-Kabi et al., "An optically pumped 2.5 μm GeSn laser on Si operating at 110 K," *Appl. Phys. Lett.*, vol. 109, no. 17, 2016, Art. no. 171105, doi: 10.1063/1.4966141.

[19] Q. M. Thai et al., "GeSn heterostructure micro-disk laser operating at 230 K," *Opt. Exp.*, vol. 26, no. 25, pp. 32500–32508, 2018, doi: 10.1364/OE.26.032500.

[20] J. Chrétien et al., "GeSn lasers covering a wide wavelength range thanks to uniaxial tensile strain," *ACS Photon.*, vol. 6, no. 10, pp. 2462–2469, 2019, doi: 10.1021/acsphotonics.9b00712.

[21] Y. Zhou et al., "Optically pumped GeSn lasers operating at 270 K with broad waveguide structures on Si," *ACS Photon.*, vol. 6, no. 6, pp. 1434–1441, Jun. 2019, doi: 10.1021/acsphotonics.9b00030.

[22] Y. Zhou et al., "Electrically injected GeSn lasers on Si operating up to 100 K," *Optica*, vol. 7, no. 8, pp. 924–928, Aug. 2020, doi: 10.1364/OPTICA.395687.

[23] H. Hong et al., "Limitation of bulk GeSn alloy in the application of a high-performance laser due to the high threshold," *Opt. Exp.*, vol. 29, no. 1, pp. 441–453, 2021, doi: 10.1364/OE.409899.

[24] D. Stange et al., "Study of GeSn based heterostructures: Towards optimized group IV MQW LEDs," *Opt. Exp.*, vol. 24, no. 2, pp. 1358–1367, 2016, doi: 10.1364/OE.24.001358.

[25] G. Abernathy et al., "Study of SiGeSn/GeSn single quantum well toward high-performance all-group-IV optoelectronics," *J. Appl. Phys.*, vol. 129, no. 9, 2021, Art. no. 093105, doi: 10.1063/5.0030230.

[26] D. Stange et al., "Quantum confinement effects in GeSn/SiGeSn heterostructure lasers," in *Proc. IEEE Int. Electron Devices Meeting*, 2017, pp. 24.2.1–24.2.4.

[27] J. Menéndez and J. Kouvetakis, "Type-I Ge/$Ge_{1-x-y}Si_xSn_y$ strained-layer heterostructures with a direct Ge bandgap," *Appl. Phys. Lett.*, vol. 85, no. 7, pp. 1175–1177, 2004, doi: 10.1063/1.1784032.

[28] B. Dutt et al., "Theoretical analysis of GeSn alloys as a gain medium for a Si-compatible laser," *IEEE J. Sel. Top. Quantum Electron.*, vol. 19, no. 5, Sep./Oct. 2013, Art. no. 1502706, doi: 10.1109/JSTQE.2013.2241397.

[29] J. Liu et al., "Tensile-strained, n-type Ge as a gain medium for monolithic laser integration on Si," *Opt. Exp.*, vol. 15, no. 18, pp. 11272–11277, Sep. 2007, doi: 10.1364/OE.15.011272.

[30] L. Liu, R. Liang, J. Wang, and J. Xu, "Investigation on the effective mass of $Ge_{1-x}Sn_x$ alloys and the transferred-electron effect," *Appl. Phys. Exp.*, vol. 8, no. 3, 2015, Art. no. 031301.

[31] H. S. Mączko, R. Kudrawiec, and M. Gladysiewicz, "Material gain engineering in GeSn/Ge quantum wells integrated with an Si platform," *Sci. Rep.*, vol. 6, 2016, Art. no. 34082, doi: 10.1038/srep34082.

[32] Z. Chen, Z. Ikonic, D. Indjin, and R. W. Kelsall, "Design optimization of tensile-strained SiGeSn/GeSn quantum wells at room temperature," *J. Appl. Phys.*, vol. 129, no. 12, 2021, Art. no. 123102.

[33] A. R. Ellis et al., "Challenges for room temperature operation of electrically pumped GeSn lasers," *Sci. Rep.*, vol. 14, no. 1, 2024, Art. no. 10318, doi: 10.1038/s41598-024-60686-3.

[34] T. Dey et al., "Molecular beam epitaxy of highly crystalline GeSnC using CBr_4 at low temperatures," *Appl. Phys. Lett.*, vol. 121, no. 12, Sep. 2022, Art. no. 122104.

[35] C. A. Stephenson, M. Gillett-Kunnath, W. A. O'Brien, R. Kudrawiec, and M. A. Wistey, "Gas source techniques for molecular beam epitaxy of highly mismatched Ge alloys," *Crystals*, vol. 6, no. 12, 2016, doi: 10.3390/cryst6120159, Art. no. 159.

[36] A. W. Arbogast et al., "Direct bandgap emission and absorption in GeCSn quantum wells," unpublished.

[37] T. Dey et al., "Epitaxy of high-quality GeCSn growth with CBr_4: Direct evidence of C and Sn incorporation," 2024, unpublished.

[38] D. Recht, F. Capasso, and M. J. Aziz, "On the temperature dependence of point-defect-mediated luminescence in silicon," *Appl. Phys. Lett.*, vol. 94, no. 25, 2009, Art. no. 251113, doi: 10.1063/1.3157277.

[39] I. A. Gulyas, C. A. Stephenson, Q. Meng, S. R. Bank, and M. A. Wistey, "The carbon state in dilute germanium carbides," *J. Appl. Phys.*, vol. 129, no. 5, 2021, Art. no. 055701.

[40] L. A. Coldren, S. W. Corzine, and M. L. Mašanović, *Diode Lasers and Photonic Integrated Circuits*, 2nd ed. Hoboken, NJ, USA: Wiley, 2012.

[41] A. B. Fallahkhair, K. S. Li, and T. E. Murphy, "Vector finite difference modesolver for anisotropic dielectric waveguides," *J. Lightw. Technol.*, vol. 26, no. 11, pp. 1423–1431, Jun. 2008.

[42] G. Timò et al., "Results on MOVPE SiGeSn deposition for the monolithic integration of III-V and IV elements in multi-junction solar cells," *Sol. Energy Mater. Sol. Cells*, vol. 224, 2021, Art. no. 111016.

[43] S. L. Chuang, *Physics of Photonic Devices*, 2nd ed. Hoboken, NJ, USA: Wiley, 2012.

[44] N.C. Chen, C. M. Lin, C. Shen, W. C. Lien, and T. Y. Lin, "Redshift of edge emission from AlGaInP light-emitting diodes and correlation with electron-hole recombination lifetime," *Opt. Exp.*, vol. 16, no. 25, pp. 20759–20773, 2008, doi: 10.1364/OE.16.020759.

[45] R. H. Yan, S. W. Corzine, L. A. Coldren, and I. Suemune, "Corrections to the expression for gain in GaAs," *IEEE J. Quantum Electron.*, vol. 26, no. 2, pp. 213–216, Feb. 1990, doi: 10.1109/3.44950.

[46] B. Gu, N. H. Kwong, and R. Binder, "Relation between the interband dipole and momentum matrix elements in semiconductors," *Phys. Rev. B*, vol. 87, no. 12, 2013, Art. no. 125301, doi: 10.1103/PhysRevB.87.125301.

[47] M. P. Polak, P. Scharoch, and R. Kudrawiec, "The electronic band structure of $Ge_{1-x}Sn_x$ in the full composition range: Indirect, direct, and inverted gaps regimes, band offsets, and the Burstein–Moss effect," *J. Phys. D: Appl. Phys.*, vol. 50, no. 19, 2017, Art. no. 195103.

[48] T. Fukushima, "Precise and fast computation of inverse Fermi–Dirac integral of order 1/2 by minimax rational function approximation," *Appl. Math. Comput.*, vol. 259, pp. 698–707, 2015.

[49] S. Gupta, "Germanium-Tin (GeSn) technology," Ph.D. dissertation, Stanford Univ.,Stanford, CA, USA, 2013.

[50] A. Rahman, M. S. Lundstrom, and A. W. Ghosh, "Generalized effective-mass approach for n-type metal-oxide-semiconductor field-effect transistors on arbitrarily oriented wafers," *J. Appl. Phys.*, vol. 97, no. 5, 2005, Art. no. 05370, doi: 10.1063/1.1845586.

[51] M. G. A. Bernard and G. Duraffourg, "Laser conditions in semiconductors," *Phys. Status Solidi B*, vol. 1, no. 7, pp. 699–703, 1961, doi: 10.1002/pssb.19610010703.

[52] P. J. A. Thiis, L. F. Tiemeijer, J. J. M. Binsma, and T. Van Dongen, "Progress in long-wavelength strained-layer InGaAs (P) quantum-well semiconductor lasers and amplifiers," *IEEE J. Quantum Electron.*, vol. 30, no. 2, pp. 477–499, Feb. 1994.

[53] T. Dey et al., "Why room temperature GeSn lasers need carbon," in *Proc. IEEE Silicon Photon. Conf.*, 2023, pp. 1–2, doi: 10.1109/SiPhotonics55903.2023.10141895.

[54] S.-H. Huang et al., "Enhanced indirect-to-direct inter-valley scattering in germanium under tensile strain for improving the population of electrons in direct valley," *J. Phys.: Condens. Matter*, vol. 30, 2018, Art. no. 465701, doi: 10.1088/1361-648X/aae50e.

[55] M. Costato, S. Fontanesi, and L. Reggiani, "Electron energy relaxation time in Si and Ge," *J. Phys. Chem. Solids*, vol. 34, no. 3, pp. 547–564, 1973, doi: 10.1016/0022-3697(73)90050-4.

[56] J. L. Oudar et al., "Femtosecond orientational relaxation of photoexcited carriers in GaAs," *Phys. Rev. Lett.*, vol. 53, no. 4, pp. 384–387, Jul. 1984, doi: 10.1103/PhysRevLett.53.384.

[57] Y. Zhou et al., "Electrically injected GeSn lasers with peak wavelength up to 2.7 μm," *Photon. Res.*, vol. 10, no. 1, pp. 222–229, 2022.

[58] M. Qi et al., "Extended defect propagation in highly tensile-strained Ge waveguides," *Crystals*, vol. 7, no. 6, 2017, Art. no. 157.

[59] C. A. Stephenson et al., "Band anticrossing in dilute germanium carbides using hybrid density functionals," *J. Electron. Mater.*, vol. 45, no. 4, pp. 2121–2126, Apr. 2016, doi: 10.1007/s11664-015-4300-9.

[60] D. Stange et al., "Short-wave infrared LEDs from GeSn/SiGeSn multiple quantum wells," *Optica*, vol. 4, pp. 185–188, 2017, doi: 10.1364/OPTICA.4.000185.

[61] D. Rainko et al., "Investigation of carrier confinement in direct bandgap GeSn/SiGeSn 2D and 0D heterostructures," *Sci. Rep.*, vol. 8, no. 1, Oct. 2018, Art. no. 15557, doi: 10.1038/s41598-018-33820-1.

[62] J. Margetis et al., "Si-Based GeSn lasers with wavelength coverage of 2-3 μm and operating temperatures up to 180 K," *ACS Photon.*, vol. 5, no. 3, pp. 827–833, Mar. 2018, doi: 10.1021/acsphotonics.7b00938.

[63] Z. I. Alferov et al., "Investigation of the influence of the AlAs-GaAs heterostructure parameters on the laser threshold current and the realization of continuous emission at room temperature," *Sov. Phys. Semicond.*, vol. 4, no. 9, pp. 1573–1575, Mar. 1971.

Authorized licensed use limited to: Texas State University. Downloaded on May 19,2025 at 15:53:30 UTC from IEEE Xplore. Restrictions apply.

[64] A. Yariv, "Scaling laws and minimum threshold currents for quantum-confined semiconductor lasers," *Appl. Phys. Lett.*, vol. 53, no. 12, pp. 1033–1035, 1988, doi: 10.1063/1.100056.
[65] T. Uenoyama, "Excitonic enhancement of optical gain in quantum wells," *Phys. Rev. B*, vol. 51, no. 15, 1995, Art. no. 10228.
[66] M. Asada, A. Kameyama, and Y. Suematsu, "Gain and intervalence band absorption in quantum-well lasers," *IEEE J. Quantum Electron.*, vol. JQE-20, no. 7, pp. 745–753, Jul. 1984.
[67] T. Takahashi, M. Nishioka, and Y. Arakawa, "Differential gain of GaAs/AlGaAs quantum well and modulation-doped quantum well lasers," *Appl. Phys. Lett.*, vol. 58, no. 1, pp. 4–6, 1991.
[68] H. Liu et al., "Long-wavelength InAs/GaAs quantum-dot laser diode monolithically grown on Ge substrate," *Nat. Photon.*, vol. 5, no. 7, pp. 416–419, Jul. 2011, doi: 10.1038/nphoton.2011.120.
[69] G. Park, O. B. Shchekin, D. L. Huffaker, and D. G. Deppe, "Low-threshold oxide-confined 1.3-μm quantum-dot laser," *IEEE Photon. Technol. Lett.*, vol. 12, no. 3, pp. 230–232, Mar. 2000, doi: 10.1109/68.826897.
[70] M. Khajavikhan et al., "Thresholdless nanoscale coaxial lasers," *Nature*, vol. 482, no. 7384, pp. 204–207, 2012, doi: 10.1038/nature10840.
[71] I. Prieto et al., "Near thresholdless laser operation at room temperature," *Optica*, vol. 2, no. 1, pp. 66–69, 2015.
[72] T. Zhou et al., "Single-mode photonic crystal nanobeam lasers monolithically grown on Si for dense integration," *IEEE J. Sel. Top. Quantum Electron.*, vol. 28, no. 3, May/Jun. 2022, Art. no. 1501906.
[73] F. Schäfer, J. Reithmaier, and A. Forchel, "High-performance GaInAs/GaAs quantum-dot lasers based on a single active layer," *Appl. Phys. Lett.*, vol. 74, no. 20, pp. 2915–2917, 1999.
[74] P. Moontragoon, N. Vukmirović, Z. Ikonić, and P. Harrison, "Electronic structure and optical properties of Sn and SnGe quantum dots," *J. Appl. Phys.*, vol. 103, no. 10, 2008.
[75] Y. Huo, "Strained Ge and GeSn band engineering for Si photonic integrated circuits," Ph.D. dissertation , Elect. Eng., Stanford Univ.,Stanford, CA, USA, 2010.
[76] M. Kondow, K. Uomi, T. Kitatani, S. Watahiki, and Y. Yazawa, "Extremely large N content (up to 10%) in GaNAs grown by gas-source molecular beam epitaxy," *J. Cryst. Growth*, vol. 164, no. 1–4, pp. 175–179, 1996.
[77] H. Kroemer, "Quasi-electric fields and band offsets: Teaching electrons new tricks (nobel lecture)," *ChemPhysChem.*, vol. 2, no. 8/9, pp. 490–499, Sep. 2001, doi: 10.1002/1439-7641(20010917)2:8/9<490.
[78] N. Holonyak, R. Kolbas, R. Dupuis, and P. Dapkus, "Quantum-well heterostructure lasers," *IEEE J. Quantum Electron.*, vol. JQE-16, no. 2, pp. 170–186, Feb. 1980.
[79] V. Reboud et al., "Lasing in group-IV materials," in *Silicon Photonics IV*, D. J. Lockwood and L. Pavesi, Eds. Berlin, Germany: Springer, 2021, pp. 105–195.
[80] P. Moontragoon, R. A. Soref, and Z. Ikonic, "The direct and indirect bandgaps of unstrained $SixGe_{1-x-y}Sn_y$ and their photonic device applications," *J. Appl. Phys.*, vol. 112, no. 7, 2012, Art. no. 073106, doi: 10.1063/1.4757414.
[81] Y.-Y. Fang et al., "Molecular-based synthetic approach to new group IV materials for high-efficiency, low-cost solar cells and Si-based optoelectronics," *J. Amer. Chem. Soc.*, vol. 130, no. 47, pp. 16095–16102, 2008, doi: 10.1021/ja806636c.
[82] G. Abernathy et al., "Study of critical optical confinement factor for GeSn-based multiple quantum well lasers," *Appl. Phys. Lett.*, vol. 121, no. 17, 2022, Art. no. 171101.
[83] Z. I. Alferov, "Nobel lecture: The double heterostructure concept and its applications in physics, electronics, and technology," *Rev. Modern Phys.*, vol. 73, no. 3, pp. 767–782, 2001, doi: 10.1103/RevModPhys.73.767.
[84] W. T. Tsang, "A graded-index waveguide separate-confinement laser with very low threshold and a narrow Gaussian beam," *Appl. Phys. Lett.*, vol. 39, no. 2, pp. 134–137, 1981.
[85] G. Sun, R. A. Soref, and H. H. Cheng, "Design of a Si-based lattice-matched room-temperature GeSn/GeSiSn multi-quantum-well mid-infrared laser diode," *Opt. Exp.*, vol. 18, no. 19, pp. 19957–19965, Sep. 2010, doi: 10.1364/OE.18.019957.
[86] G. Sun, R. A. Soref, and H. H. Cheng, "Design of an electrically pumped SiGeSn/GeSn/SiGeSn double-heterostructure midinfrared laser," *J. Appl. Phys.*, vol. 108, no. 3, 2010, doi: 10.1063/1.3467766.
[87] S. Q. Lim et al., "Remote plasma-enhanced chemical vapor deposition of GeSn on Si: Material and defect characterization," *J. Appl. Phys.*, vol. 133, no. 23, 2023, Art. no. 235302.
[88] Y.-Y. Fang et al., "Perfectly tetragonal, tensile-strained Ge on $Ge_{1-y}Sn_y$ buffered Si (100)," *Appl. Phys. Lett.*, vol. 90, no. 6, 2007, Art. no. 061915, doi: 10.1063/1.2472273.
[89] S. Takeuchi et al., "Growth of highly strain-relaxed $Ge_{1-x}Sn_x$/virtual Ge by a Sn precipitation controlled compositionally step-graded method," *Appl. Phys. Lett.*, vol. 92, no. 23, Jun. 2008, Art. no. 231916, doi: 10.1063/1.2945629.
[90] J. Margetis et al., "All group-IV SiGeSn/GeSn/SiGeSn QW laser on Si operating up to 90 K," *Appl. Phys. Lett.*, vol. 113, no. 22, 2018, Art. no. 221104.
[91] J. Liu, L. C. Kimerling, and J. Michel, "Monolithic Ge-on-Si lasers for large-scale electronic–photonic integration," *Semicond. Sci. Technol.*, vol. 27, no. 9, 2012, Art. no. 094006.
[92] S. Gupta, D. Nam, J. Vuckovic, and K. Saraswat, "Room temperature lasing unraveled by a strong resonance between gain and parasitic absorption in uniaxially strained germanium," *Phys. Rev. B*, vol. 97, no. 15, 2018, Art. no. 155127, doi: 10.1103/PhysRevB.97.155127.
[93] G. Childs, S. Brand, and R. A. Abram, "Intervalence band absorption in semiconductor laser materials," *Semicond. Sci. Technol.*, vol. 1, no. 2, pp. 116–120, 1986.
[94] S. Dominici, H. Wen, F. Bertazzi, M. Goano, and E. Bellotti, "Numerical study on the optical and carrier recombination processes in GeSn alloy for E-SWIR and MWIR optoelectronic applications," *Opt. Exp.*, vol. 24, no. 23, pp. 26363–26381, 2016, doi: 10.1364/OE.24.026363.
[95] S. Dominici, H. Wen, F. Bertazzi, M. Goano, and E. Bellotti, "Numerical evaluation of Auger recombination coefficients in relaxed and strained germanium," *Appl. Phys. Lett.*, vol. 108, 2016, Art. no. 211103, doi: 10.1063/1.4952720.
[96] J.-X. Shen, X. Zhang, S. Das, E. Kioupakis, and C. G. Van de Walle, "Unexpectedly strong auger recombination in halide perovskites," *Adv. Energy Mater.*, vol. 8, no. 30, 2018, Art. no. 1801027, doi: 10.1002/aenm.201801027.
[97] J. I. Pankove, *Optical Processes in Semiconductors*. New York, NY, USA: Dover, Dec. 2012.

Md. Shamim Reza was born in Bangladesh in 1991. He received the B.S. degree in physics from the University of Dhaka, Dhaka, Bangladesh, in 2015, the M.S. degree in physics from the University of Louisville, Louisville, KY, USA, in 2017, and the Ph.D. degree in materials science, engineering, and commercialization from Texas State University, San Marcos, TX, USA, in 2022. He is currently a Technology Development Epitaxy Engineer with Intel Corporation, Hillsboro, OR, USA. He has authored or coauthored six journal and seven conference papers. His research interests include molecular beam epitaxy of Group IV materials, EPI growth of doped polysilicon on MOCVD, silicon photonics, and materials characterization. He was the recipient of Doctoral Research Fellowships in 2021 and a Departmental Division Award in 2024 for outstanding work with Intel Corporation.

Tuhin Dey was born in Sylhet, Bangladesh, in 1988. He received the B.S. and M.S. degrees in electrical and electronic engineering from American International University-Bangladesh, Dhaka, Bangladesh, in 2013, and the Ph.D. degree in materials science, engineering and commercialization program from Texas State University, San Marcos, TX, USA, in 2023. From 2013 to 2017, he was a Faculty Member with the Shahjalal University of Science and Technology, Sylhet, Bangladesh. He is currently with Lam Research. His research interests include molecular beam epitaxy of group-IV semiconductors, silicon photonics, group-IV heterostructures, and thin film growth and characterization. He was the recipient of the Eramus Mundas scholarship in 2017 and a doctoral merit fellowship in 2018.

Authorized licensed use limited to: Texas State University. Downloaded on May 19,2025 at 15:53:30 UTC from IEEE Xplore. Restrictions apply.

Augustus W. Arbogast was born in Texas in 1994. He received the B.S. and M.S. degrees in physics from Texas State University, San Marcos, TX, USA, in 2019 and 2022, respectively. He is currently a Research Assistant with Texas State University. He has authored or coauthored two journal papers and three conference papers.

Qian Meng received the B.S. degree in microelectronics from Sichuan University, Chengdu, China, and the M.S. and Ph.D. degrees in electrical and computer engineering from the University of Texas at Austin, Austin, TX, USA. She is currently with the Microelectronics Research Center and the Electrical and Computer Engineering Department, University of Texas at Austin, co-advised by Prof. Seth Bank and Prof. Mark Wistey. Her research interests include understanding the fundamental properties of highly mismatched alloys (HMAs) grown by molecular beam epitaxy (MBE).

Seth R. Bank (Fellow, IEEE) received the B.S. degree in electrical engineering from the University of Illinois at Urbana-Champaign (UIUC), Urbana, IL, USA, in 1999, and the M.S. and Ph.D. degrees in electrical engineering from Stanford University, Stanford, CA, USA, in 2003 and 2006, respectively. At UIUC, he studied the fabrication of InGaP–GaAs and InGaAs–InP HBTs. His Ph.D. research interests include the MBE growth, fabrication, and device physics of long-wavelength VCSELs, and low-threshold edge-emitting lasers in the GaInNAs (Sb)–GaAs material system. In 2006, he was a Postdoctoral Scholar with the University of California, Santa Barbara, CA, USA, where his research centered on the growth of metal–semiconductor hetero- and nano-structures (e.g., ErAs nanoparticles in GaAs). In 2007, he joined the University of Texas at Austin, Austin, TX, USA, where he is currently an Associate Professor of electrical and computer engineering and the holder of the fifth Temple Foundation Endowed Faculty Fellowship. He has coauthored more than 175 papers and presentations in his research field, which include the MBE growth of novel heterostructures and nanocomposites and their device applications. Dr. Bank was the recipient of the 2010 Young Investigator Program Award from ONR, 2010 NSF CAREER Award, 2009 Presidential Early Career Award for Scientists and Engineers (PECASE) nominated by ARO, 2009 Young Investigator Program Award from AFOSR, 2009 Young Scientist Award from the International Symposium on Compound Semiconductors, 2008 DARPA Young Faculty Award, 2008 Young Investigator Award from the North American MBE Meeting, and several best paper awards.

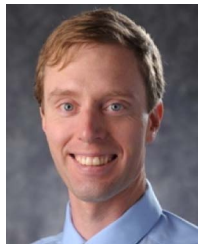

Mark A. Wistey (Senior Member, IEEE) received the B.S. degree in electrical engineering from Montana State University, Bozeman, MT, USA, in 1995, and the M.S. and Ph.D. degrees in electrical engineering from Stanford University, Stanford, CA, USA, in 2000 and 2005, respectively. He was a Visiting Scholar with Stanford University in 2005; a Postdoctoral Research Associate with Arizona State University, in 2006; and a Postdoctoral Research Scholar with the University of California, Santa Barbara, Santa Barbara, CA, USA, from 2007 to 2009. From 2009 to 2017, he was an Assistant Professor of electrical engineering with University of Notre Dame, Notre Dame, IN, USA. Since 2017, he has been an Associate Professor of physics with Texas State University, San Marcos, TX, USA. He has coauthored two book chapters, 88 journal articles, 151 conference papers, and one patent. His research interests include silicon photonics and integrated optoelectronics, high efficiency solar cells, heterogeneous integration, molecular beam epitaxy, low energy electronics, and devices and materials for renewable energy. Dr. Wistey was the recipient of the MBE Young Investigator Award in 2013, Ross Tucker Award for semiconductor materials in 2004, and Outstanding Student Paper Award at the 2003 North American Molecular Beam Epitaxy conference.

Authorized licensed use limited to: Texas State University. Downloaded on May 19,2025 at 15:53:30 UTC from IEEE Xplore. Restrictions apply.